Research on the Catalytic Behavior of Ni-VC/SiO2 Catalyst for Methane Cracking

Shoufu Li * and Aizhong Ding

Posted Date: 19 December 2024

doi: 10.20944/preprints202412.1624.v1

Keywords: Vanadium-based catalysts; Methane cracking; Hydrogen energy; Biogas; Degree of graphitization

Article

Research on the Catalytic Behavior of Ni-VC/SiO_2 Catalyst for Methane Cracking

Shoufu Li *, Aizhong Ding, Zhaoyong bian and Yuanyan Xuan

College of Water Sciences, Beijing Normal University,No.19 Xinjiekouwai Street, Beijing 100875,China
* Correspondence: 202321470010@mail.bnu.edu.cn

Abstract: With the growth of global energy demand and the reduction of fossil fuels, the search for clean energy has become particularly urgent. Hydrogen energy, due to its cleanliness and high efficiency, is regarded as an ideal alternative energy source. Methane catalytic cracking technology, as an effective way to produce hydrogen, has significant economic and environmental value.This study focuses on the application of vanadium-based catalysts in biogas cracking for hydrogen production. Vanadium-based catalysts have shown great potential in the dehydrogenation of hydrocarbons due to their cost-effectiveness, environmental compatibility, high catalytic activity, and stability. An innovative one-step method was used to prepare Ni-VC/TiO2 composite catalysts, and the impact of vanadium carbide (VC) content on the performance of the catalyst was studied. The addition of VC not only optimized the catalyst's active surface area but also enhanced its conductivity and electron transfer capability, thereby improving catalytic efficiency.Experimental results indicate that an increase in VC content leads to a decrease in the specific surface area and pore volume of the catalyst, but an increase in pore size, which is beneficial for the adsorption and diffusion of gas molecules. Moreover, the reaction temperature has a significant effect on the performance of the catalyst: at 500°C, the 10Ni-5VC/TiO2 catalyst exhibited the highest stability and hydrogen production rate. However, at higher temperatures, the methane conversion rate and hydrogen yield will drop sharply due to the increased graphitization of coke, which accelerates the deactivation of the catalyst.Through regeneration experiments, we found that using CO2 as an activator at 600°C can effectively restore the activity of the catalyst. However, as the number of regenerations increases, the performance of the catalyst gradually decreases, which is related to the increase in Ni grain size and the formation of surface amorphous coke. SEM and TEM analysis showed that coke mainly exists in the form of filamentous carbon, which affects the long-term stability of the catalyst.

Keywords: vanadium-based catalysts; methane cracking; hydrogen energy; biogas; degree of graphitization

1. Introduction

With the rapid development of the global economy, energy demand continues to soar. The over-reliance on and consumption of traditional fossil fuels not only accelerates the depletion of resources but also brings about serious environmental issues. Faced with the increasingly severe energy crisis and environmental pollution, the development of clean, sustainable energy technology has become a global focus. Hydrogen energy, as a clean, efficient, and renewable energy carrier, is of great significance for promoting the transformation of energy structures and reducing greenhouse gas emissions.

Methane, as the main component of natural gas, is a rich hydrocarbon resource. Catalytic methane decomposition for hydrogen production (CMD) is considered a promising hydrogen production process due to its simple process, easy separation of products, and no CO_x production. However, the C-H bond in methane molecules is very stable and difficult to activate and decompose.

 doi:10.20944/preprints202412.1624.v1

Therefore, developing efficient catalysts to promote the catalytic decomposition reaction of methane is key to the commercial application of this technology.Nickel-based catalysts have been widely used in the dehydrogenation or hydrogenation reactions of hydrocarbons due to their low cost, environmental friendliness, and superior catalytic performance. However, pure nickel catalysts are prone to sintering and coking at high temperatures, leading to a rapid decline in catalytic activity, which limits their industrial application in methane catalytic decomposition. To address this issue, researchers have improved the performance of catalysts by controlling preparation methods, optimizing reaction processes, and adding metal dopants, aiming to synthesize low-cost, high-activity methane decomposition catalysts for hydrogen production.

Vanadium, as an important metal element, has multiple oxidation states and good catalytic activity. The introduction of vanadium can not only improve the conductivity and electron transfer capability of the catalyst, enrich the number of active sites, but also enhance the catalytic performance by changing the crystal structure of the catalyst. In addition, doping vanadium can affect the interaction between the metal and the support, thereby suppressing the agglomeration and sintering of metal particles during the reaction process, and improving the thermal stability and service life of the catalyst.This study used commercial nano titanium dioxide (TiO_2) as a carrier to prepare Ni/TiO2 catalysts by the impregnation method and systematically studied the effects of calcination temperature, metal loading, and reaction temperature on the performance of methane catalytic decomposition. At the same time, by introducing vanadium carbide (VC) as a dopant into the Ni/TiO_2 catalyst, a one-step method was used to prepare Ni-VC/TiO_2 composite catalysts, and the effects of VC content and reaction temperature on the catalyst structure and methane decomposition performance were investigated. In addition, using titanium tetraethoxide (TEOS) as a titanium source, mesoporous nano titanium dioxide particles (MSN) with high specific surface area and large pore volume were synthesized by the template method, and metal Ni was loaded to further study the effects of metal loading and reaction temperature on the performance of the catalyst.

The findings of this study provide important theoretical basis and technical support for the design and preparation of methane catalytic decomposition catalysts for hydrogen production, which has significant scientific significance and application value for promoting the commercial development of hydrogen energy.

Experimental Section

2.1. Catalyst Preparation

A certain amount of nickel nitrate hexahydrate ($Ni(NO3)_2{\cdot}6H_2O$) is dissolved in 25 milliliters of water. Then, a certain amount of vanadium carbide (VC) and 2 grams of nanometer titanium dioxide (TiO_2) are weighed and slowly added to the above solution. At room temperature, the solution is stirred for 24 hours using a magnetic stirrer for impregnation. Afterward, the prepared solution is placed in a rotary evaporator to evaporate the solvent, and then the resulting solution is transferred to an oven for drying. The dried sample is ground into a powder and collected. These uniformly mixed powder samples are transferred to a ceramic boat and placed in the temperature-controlled area of a carbonization furnace. Through this process, we ultimately obtained a catalyst named nNi-xVC/TiO_2, where n and x represent the mass percentage of nickel atoms and vanadium carbide to titanium dioxide before mixing, respectively.

2.2. Characterization Methods

A physical adsorption apparatus model JW-BK200A is used to perform adsorption-desorption experiments at a nitrogen environment of 77 K to evaluate the structural characteristics of the samples. Before the adsorption experiment, the samples are pretreated under vacuum at 300 °C for 3 hours to remove adsorbed gases and moisture from the samples. Then, the specific surface area and pore size distribution of the samples are calculated using the Brunauer-Emmett-Teller (BET) method and the Barrett-Joyner-Halenda (BJH) method, respectively. The X-ray diffraction (XRD) patterns of the samples are obtained using a D/MAX-2400 X-ray diffractometer under Cu Kα radiation

 doi:10.20944/preprints202412.1624.v1

conditions of 30 kV and 30 mA. Hydrogen temperature-programmed reduction (H2-TPR) analysis of the catalyst is conducted using a PCA-1200 chemical adsorption analyzer. Finally, the morphology and structure of the samples after the methane catalytic cracking reaction are analyzed using a Quanta450 scanning electron microscope (SEM) and a JEM-2000EX transmission electron microscope (TEM) from FEI Company, USA.

2.3. Methane Catalytic Cracking Experiment

The methane catalytic cracking experiment was carried out in an atmospheric pressure fixed-bed reactor with a diameter of 8 millimeters. First, 0.2 grams of catalyst were placed in the temperature-controlled zone of the reactor. The reactor was heated to the set reaction temperature under a nitrogen atmosphere (40 mL/min), and then the gas was switched to a mixture of 10 mL/min methane and 40 mL/min nitrogen. After the reaction was stabilized for 5–10 minutes, the products were collected and analyzed for their composition online using a GC7890II gas chromatograph. The performance of the catalyst was evaluated based on the methane conversion rate and the carbon yield, with the calculation formulas as follows:

Methane Conversion Rate:

$C_{CH4}=(F_{CH4,in}-F_{CH4,out})/F_{CH4,in}\times 100\%$

Carbon Yield:

Carbon yield (g_C/g_{Ni}) = Mass of coke deposited/ Mass of metal in the catalyst × 100%

2. Study on the Catalytic Cracking Behavior of Methane Over Ni-VC/TiO2 Catalyst

3.1. The Impact of VC Content on the Catalyst Structure and Methane Cracking

Performance In the catalytic process of methane cracking for hydrogen production, the efficiency of the catalyst is significantly affected by the crystallite size of the metal particles; the larger the crystallite size, the faster the deactivation rate of the catalyst. Using the Scherrer equation, the average size of nickel (Ni) particles before and after the reaction for 10Ni-xVC/TiO2 catalysts with different loadings of vanadium carbide (VC) was calculated, and the relevant results are listed in Table 1. It was observed that with the increase in VC content, the size of Ni particles in the catalyst increased both before and after the reaction. This phenomenon may be due to the spatial constraints of the carrier leading to a reduction in the dispersion of the crystallites.

Table 1. Average particle tize of nickel particles before and after reaction of catalyst with different.

Samples	Fresh (nm)	Spent (nm)	Reaction time (min)
10Ni	16.7	17.0	200
10Ni-1VC	11.2	17.2	250
10Ni-3VC	16.5	20.3	410
10Ni-5VC	23.5	24.1	450
10Ni-10VC	31.2	31.7	330

Additionally, in the process of catalytic methane cracking for hydrogen production, the optimal metal particle size for nickel-based catalysts is 23nm, which coincides with the nickel particle size of the 10Ni-5VC/TiO2 catalyst in this study. Compared with the catalyst in its initial state, the Ni/TiO2

 doi:10.20944/preprints202412.1624.v1

catalyst only saw a 0.1nm increase in nickel crystallite size after 200 minutes of reaction. However, within a reaction time of 450 minutes, the nickel crystallite size of the 10Ni-5VC/TiO2 catalyst only slightly increased from 23.5nm to 24.1nm, showing the smallest crystallite growth in vanadium-containing catalysts. This indicates that an appropriate amount of VC doping can alter the interaction between the metal and the support, affecting the agglomeration mechanism of nickel crystallites, thereby effectively inhibiting the growth of nickel microcrystals.

Table 2 presents the structural characteristics of catalysts with different VC contents. The data from the table show that as the VC content increases, the specific surface area and pore volume of the 10Ni-xVC/TiO2 (x=1, 3, 5, 10) series of catalysts are significantly reduced. Compared with the 10Ni/TiO2 catalyst without VC doping, the addition of VC resulted in a decrease in the specific surface area of the prepared catalyst, but an increase in pore volume and pore size. The reasons for this phenomenon may include: on one hand, the loading of the metal active components on the surface of the carrier or the blockage within the pores, leading to a reduction in surface area; on the other hand, the reduction reaction between nickel oxides and vanadium carbide may have disrupted the skeleton structure of the carrier material, causing small particles to aggregate and form a porous structure with larger pore volume and pore size.

Table 2. Textural properties of the catalysts with different VC contents.

Sample	SBET (m^2/g)	Vt (cm^3/g)	Dave (nm)
10Ni/TiO2	184.8	0.88	15.5
10Ni-1VC/TiO2	182.7	1.40	25.5
10Ni-3VC/TiO2	170.9	1.32	25.2
10Ni-5VC/TiO2	146.7	1.32	25.5
10Ni-10VC/TiO2	143.7	1.21	25.7

3.2. The Effect of Reaction Temperature on the Performanc of Methane Cracking

According to previous studies, the reaction temperature significantly affects the activity and stability of the catalyst, and it is also an important factor affecting the degree of metal particle agglomeration and the form of carbon deposition on the catalyst surface. Therefore, the 10Ni-5VC/TiO2 catalyst was selected to study the impact of reaction temperature on the structure of the vanadium-doped catalyst and its performance in catalytic methane cracking.

Figure 1 shows the XRD patterns of the 10Ni-5VC/TiO2 catalyst before and after the reaction at different reaction temperatures. Compared with the catalyst before the reaction, only the diffraction peaks of graphite carbon and metallic nickel were observed after the reaction. The diffraction peaks at 2θ = 26.4° and 43.5° are attributed to the C(002) and C(101) crystal planes of graphite carbon, respectively, which is the result of a large amount of coke formation from catalytic methane cracking. The intensity ratio of these two peaks, C(101)/C(002), reflects the degree of order in the graphite carbon layer; the lower the ratio, the higher the structural order.

 doi:10.20944/preprints202412.1624.v1

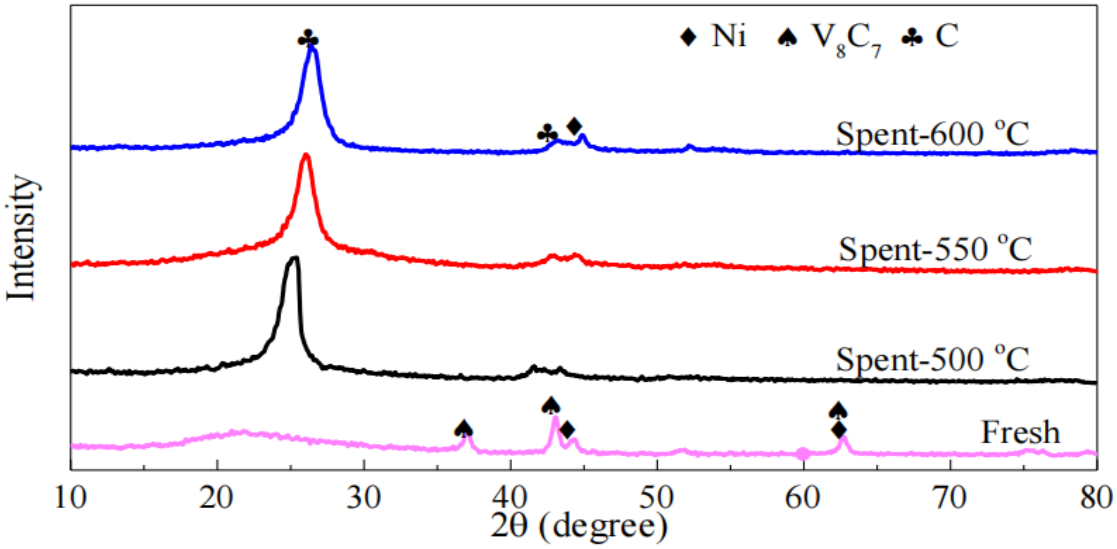

Figure 1. XRD patterns of the catalysts with different reaction temperatures.

The catalytic performance of the 10Ni-5VC/TiO2 catalyst in methane cracking at different reaction temperatures is shown in Figure 2. As can be seen from Figure 2, under different reaction temperatures, the methane conversion rate shows the same trend of increasing first and then decreasing. It is believed that the increase in catalyst activity in the methane cracking reaction is due to the need to go through an induction period before reaching the maximum value. Due to the smaller crystallite size of the nanometer catalyst, the initial stage of the reaction gradually forms metal active sites of the appropriate size. However, as the reaction proceeds, rapid coking on the surface of the catalyst buries the active sites, and the agglomeration and sintering of metal particles lead to a decrease in catalytic activity. Moreover, an increase in reaction temperature is conducive to the improvement of methane conversion rate, but at higher temperatures, the methane conversion rate drops sharply, and the hydrogen production decreases accordingly. At a reaction temperature of 500°C, the 10Ni-5VC/TiO2 catalyst exhibits the best catalytic stability, with the methane conversion rate remaining around 14.2% after 2300 minutes of reaction.

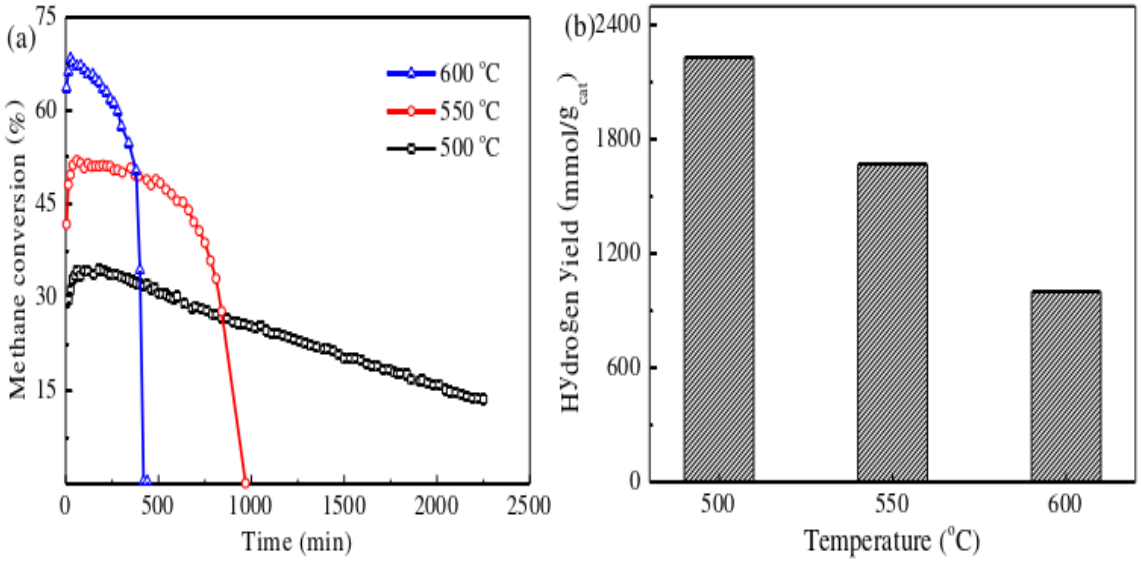

Figure 2. Methane converTion (a) and hydrogen yield (b) of the catalysts with different reaction temperatures.

 doi:10.20944/preprints202412.1624.v1

To further investigate the cause of catalyst deactivation, the surface morphology of the post-reaction catalyst was analyzed. It was observed that with the increase in reaction temperature, the diameter and length of the filamentous carbon decreased. Due to the large randomness in the growth direction of the filamentous carbon and their interweaving nature, accurately measuring their true length is relatively difficult. However, statistical data on the diameter distribution indicate that at reaction temperatures of 500°C, 550°C, and 600°C, the average diameter of the filamentous carbon decreased from 95 nm to 65 nm and then to 33 nm. This can be attributed to the pseudo-liquid transformation and fragmentation of metal particles. Therefore, the reduction in filament length and diameter at high temperatures accelerates the deactivation of the catalyst.

The experiment used Raman spectroscopy to examine the effect of reaction temperature on the graphitization degree of carbon deposition on the catalyst surface. As shown in Figure 3, all samples exhibited absorption peaks around 1340 cm-1 and 1580 cm-1, attributed to the D-band and G-band, respectively. The D-band is mainly caused by structural defects in graphite, while the G-band is due to the in-plane stretching vibration of carbon-carbon in graphite layers. A shoulder peak (D') of the G-band was observed at 1615 cm-1, and the D' peak is also considered to be related to defects in graphite and other carbonaceous species. Since the intensity of the D-band increases with the degree of structural defects in graphite, the ratio of the intensities of the D-band to the G-band, ID/IG, is commonly used to evaluate the graphitization degree and crystallinity of the deposited carbon on the catalyst. The lower this value, the higher the graphitization degree of the coke. As the reaction temperature increases, the ID/IG value decreases, indicating an increase in the orderliness of the coke after the reaction. It can be seen that the reaction temperature has a significant effect on the graphitization degree of the coke, and an increase in reaction temperature leads to an increase in the graphitization degree of the coke produced by cracking.

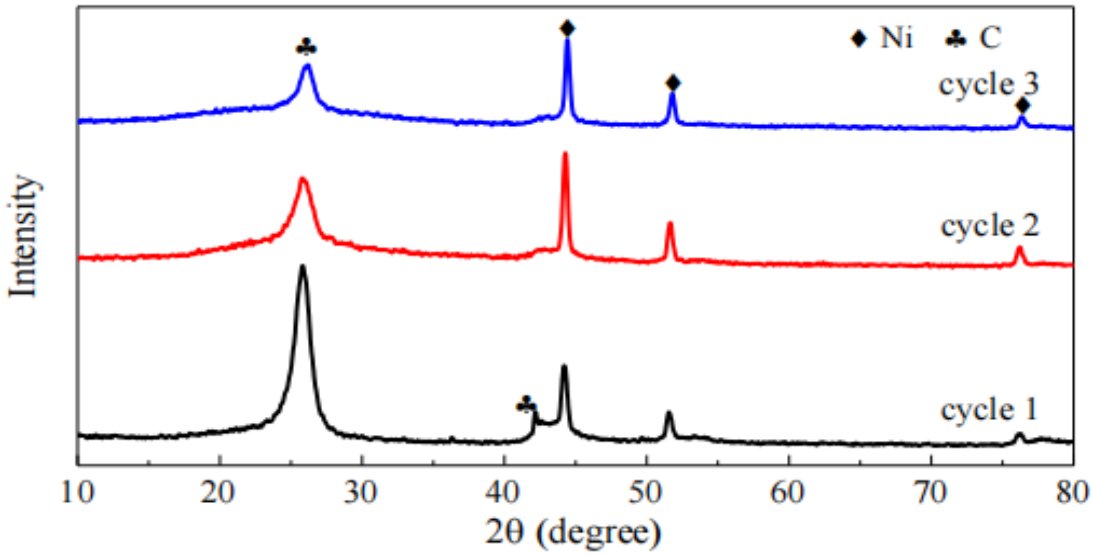

Figure 3. XRD patterns of the spent Ni-VC/TiO2 catalyst after different regeneration cycles.

3.3. Catalysts Regeneration

Based on the previous findings, under the reaction conditions of 550°C, 30Ni-VC/TiO2 exhibited relatively good reactivity and stability. The lower reaction temperature is beneficial for the growth of filamentous carbon, which can yield higher rates of hydrogen production and filamentous carbon recovery. However, during the reaction process, the carbon formed covers the active centers, leading to catalyst deactivation. To explore the regeneration capability of the post-reaction catalyst, the 30Ni-VC/TiO2 was chosen as the subject for regeneration studies. The regeneration steps are as follows:

Using CO2 as an activating agent, CO2 is introduced into a fixed-bed reactor at atmospheric pressure and 600°C. The composition of the regenerated gas is monitored online by gas chromatography until no CO is produced. The CO2 valve is then closed, and the reactor is purged

 doi:10.20944/preprints202412.1624.v1

with nitrogen until the temperature drops to 550°C. The methane valve is then opened to conduct the methane cracking experiment again. The regeneration cycles are repeated until the catalyst is completely deactivated.

Figure 4 shows the XRD patterns of the 30Ni/TiO2 catalyst after different cycles of regeneration reactions. The diffraction peaks at 2θ of 26.4° and 43.5° are attributed to the C(002) and C(101) crystal planes, respectively, confirming the formation of coke during the methane cracking reaction. Comparisons reveal that the intensity of the Ni diffraction peaks increases after different cycles of reactions, indicating an enlargement of Ni crystallites. For the carbon diffraction peaks, their intensity gradually decreases, which is consistent with the results of the methane catalytic cracking experiments. Using the Scherrer equation, the average particle sizes of nickel in the catalyst after three cycles were calculated to be 20.0 nm, 22.3 nm, and 23.1 nm, respectively. This increase in Ni crystallite size may be one of the reasons for the reduced reactivity.

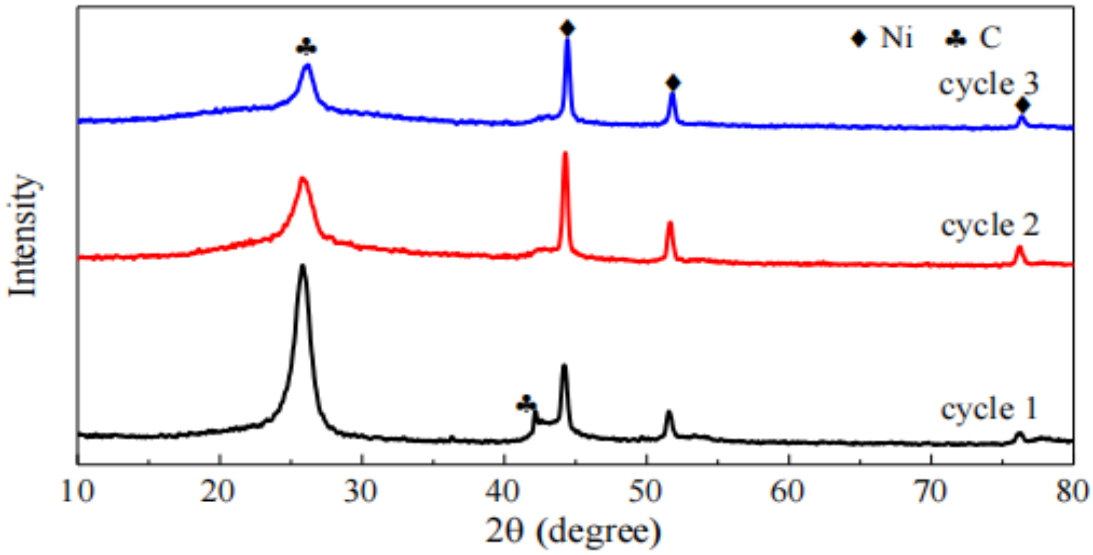

Figure 4. XRD patterns of the spent Ni-VC/TiO2 catalyst after different regeneration cycles.

As can be seen from Figure 5, although the regeneration process can restore the reactivity of the catalyst, with the increase in the number of cracking cycles, the methane conversion rate and reaction stability of the catalyst show a clear trend of decline. This may be attributed to the regeneration experiment conducted on the catalyst at 600°C, which causes sintering of the Ni particles, leading to changes in the catalyst's structure and performance.

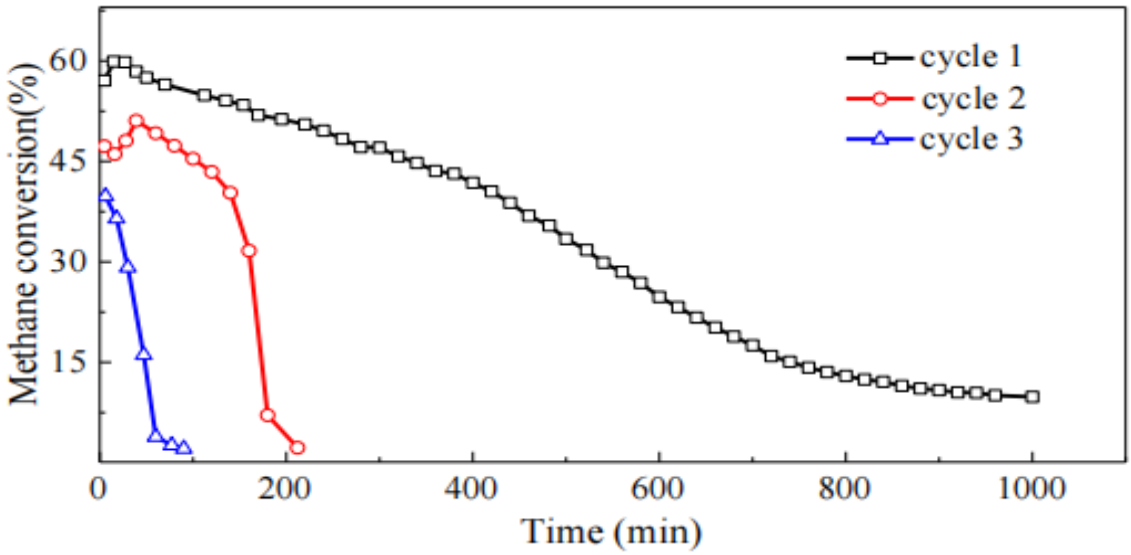

 doi:10.20944/preprints202412.1624.v1

Figure 5. Methane converTion of the Ni/TiO2 catalyst after succesTive regeneration cycles.

Using SEM for surface morphology analysis of the post-reaction catalyst, it was observed that after three regeneration cycles, the catalyst surface was covered with interwoven filamentous carbon. The formation of this filamentous carbon can maintain the catalyst's activity over a longer period, preventing the active centers from being completely covered. However, with the increase in the number of cracking-regeneration cycles, the amount of filamentous carbon formed decreases, becoming shorter and thinner, and there is a significant agglomeration phenomenon. This may be related to the sintering and grain growth of Ni particles during the regeneration process. Additionally, after three regeneration cycles, a large amount of amorphous carbon appeared on the surface of the catalyst, which may be one of the reasons for the decline in catalyst activity.

4. Conclusions

To enhance the activity and durability of the Ni/TiO2 catalyst, this study employed a one-step method to prepare a composite catalyst by mixing the metal active components with vanadium carbide impregnation, thereby avoiding an additional reduction step and simplifying the preparation process. This study also prepared a series of 10Ni-xVC/TiO2 catalysts with different VC doping amounts and studied the impact of reaction temperature on catalyst performance and the efficiency of catalytic methane cracking. The main findings are as follows:

The metal-loaded catalyst was prepared by a one-step method using the traditional impregnation technique, by mixing vanadium carbide with metal precursors. This Ni-VC/TiO2 catalyst has a cylindrical pore structure with a mesostructure, and the pore size is mainly concentrated between 20 and 40 nm. The addition of vanadium carbide significantly improved the performance of the Ni/TiO2 catalyst. The activity of the catalyst first increased and then decreased with the increase of VC content. In particular, the 10Ni-5VC/TiO2 catalyst maintained a methane conversion rate of about 14.2% after 2300 minutes of reaction at 500°C. The addition of VC effectively slowed down the growth of Ni microcrystals during the catalytic methane cracking process. The 10Ni-5VC/TiO2 catalyst had a particle size of 23.7nm before the reaction, which is very close to the optimal particle size of Ni particles (23nm) in the catalytic methane cracking experiment. After 450 minutes of reaction, the size of the Ni crystallites only increased to 24.0nm, showing the smallest growth rate. The reaction temperature has a significant impact on the activity and stability of the catalyst. Lower temperatures help to improve the stability of methane cracking, which may be due to the formation of longer and thicker filamentous carbon on the surface of the catalyst after the reaction. High temperatures, on the other hand, accelerate the deactivation of the catalyst. Raman spectroscopy analysis showed that the reaction temperature significantly affected the graphitization degree of the carbon fibers, and the graphitization degree of the carbon produced by methane cracking increased with the rise in temperature.

The post-reaction Ni-VC/TiO2 catalyst was analyzed using a scanning electron microscope (SEM) and a transmission electron microscope (TEM). The analysis showed that the coke produced by the Ni-VC/TiO2 catalyst mainly presented as "octopus-like" filamentous carbon. These filamentous carbons can serve as carriers for the growth of metal particles in the initial stage. As the filamentous carbon grows, they help to disperse metal particles, thereby improving catalytic performance. However, at high temperatures, the type of carbon produced by methane cracking changed, leading to a decrease in reaction stability. Using CO2 as an activator, a cracking-regeneration cycle experiment was conducted on the post-reaction catalyst in a fixed-bed reactor under atmospheric pressure. The experimental results showed that with the increase in the number of regeneration cycles, the methane conversion rate and reaction stability significantly decreased, mainly due to the growth of Ni crystallites after regeneration and the formation of a large amount of amorphous coke on the surface of the catalyst.

 doi:10.20944/preprints202412.1624.v1

References

1. Meiliefiana M., Nakayashiki T., Yamamoto E., et al. One-Step Solvothermal Synthesis of Ni Nanoparticle Catalysts Embedded in ZrO2 Porous Spheres to Suppress Carbon Deposition in Low-Temperature Dry Reforming of Methane [J]. Nanoscale Research Letters, 2022, 47.
2. Velev O. D., Jede T. A., Lobo R. F., et al. Porous silica via colloidal crystallization [J]. Nature, 1997, 389: 447-448.
3. Li H., Qiu Y., Wang C., et al. Nickel catalysts supported on ordered mesoporous SiC materials for CO2 reforming of methane [J]. Catalysis Today, 2018, 317: 76-85.
4. Wang N., Shen K., Huang L., et al. Facile Route for Synthesizing Ordered Mesoporous Ni–Ce–Al Oxide Materials and Their Catalytic Performance for Methane Dry Reforming to Hydrogen and Syngas [J]. ACS Catalysis, 2013, 3(7): 1638-1651.
5. Hossain M. K., Hossain S., Ahmed M. H., et al. A Review on Optical Applications, Prospects, and Challenges of Rare-Earth Oxides [J]. ACS Applied Electronic Materials, 2021, 3(9): 3715-3746.
6. Patil A. S., Patil A. V., Dighavkar C. G., et al. Synthesis techniques and applications of rare earth metal oxides semiconductors: A review [J]. Chemical Physics Letters, 2022, 796: 139555.
7. Victor Z., Larisa E., Rina S., et al. Preparation and Mechanical Characteristics of Multicomponent Ceramic Solid Solutions of Rare Earth Metal Oxides Synthesized by the SCS Method [J]. Ceramics, 2023, 6(2): 1017-1030.
8. Hossain M. K., Rubel M. H. K., Akbar M. A., et al. A review on recent applications and future prospects of rare earth oxides in corrosion and thermal barrier coatings, catalysts, tribological, and environmental sectors [J]. Ceramics International, 2022, 48(22): 32588- 32612.
9. Rui-jie L. I., Ju-ping Z., Jian S. H. I., et al. Regulation of metal-support interface of Ni/CeO2 catalyst and the performance of low temperature chemical looping dry reforming of methane [J]. Journal of Fuel Chemistry and Technology, 2022, 50(11): 1458-1470.
10. Jiang C., Loisel E., Cullen D. A., et al. On the enhanced sulfur and coking tolerance of NiCo-rare earth oxide catalysts for the dry reforming of methane [J]. Journal of Catalysis, 2020, 393: 215-229.
11. Xu L., Liu W., Zhang X., et al. Ni/La2O3 Catalysts for Dry Reforming of Methane: Insights into the Factors Improving the Catalytic Performance [J]. ChemCatChem, 2019, 11(12): 2887-2899.
12. Blal M., Belasri A., Benatillah A., et al. Assessment of solar and wind energy as motive for potential hydrogen production of Algeria country; development a methodology for uses hydrogen-based fuel cells [J]. International Journal of Hydrogen Energy, 2018, 43: 9192- 9210.
13. Xiaoguang S., Jia C., Yanxing C., et al. New Design and Construction of Hierarchical Porous Ni/SiO2 Catalyst with Anti-sintering and Carbon Deposition Ability for Dry Reforming of Methane [J]. ChemistrySelect, 2022, 7(36).
14. Wang J., Kim J., Choi S., et al. A Review of Carbon-Supported Nonprecious Metals as Energy-Related Electrocatalysts [J]. Small Methods, 2020, 4(10).
15. Bernal S., Blanco E., Botana K. J., et al. Preparation of some rare earth oxide supported rhodium catalysts: Study of the supports [J]. Materials Chemistry and Physics, 1987, 17: 433-443.
16. Zhang Y., Jung I.-H. Critical evaluation of thermodynamic properties of rare earth sesquioxides (RE = La, Ce, Pr, Nd, Pm, Sm, Eu, Gd, Tb, Dy, Ho, Er, Tm, Yb, Lu, Sc and Y) [J]. Calphad, 2017, 58: 169-203.
17. Sutthiumporn K., Kawi S. Promotional effect of alkaline earth over Ni-La2O3 catalyst for CO2 reforming of CH4: Role of surface oxygen species on H2 production and carbon suppression [J]. International Journal of Hydrogen Energy, 2011, 36 (22): 14435-14446.
18. Al-Fatesh A. S. Promotional effect of Gd over Ni/ Y2O3 catalyst used in dry reforming of CH4 for H2 production [J]. International Journal of Hydrogen Energy, 2017, 42 (30): 18805- 18816.
19. Bahari M. B., Setiabudi H. D., Trinh Duy N., et al. Insight into the influence of rare-earth promoter (CeO2, La2O3, Y2O3, and Sm2O3) addition toward methane dry reforming over Co/mesoporous alumina catalysts [J]. Chemical Engineering Science, 2020, 228: 115967.
20. Wang Y., Li L., Wang Y., et al. Highly Carbon-Resistant Y Doped NiO-ZrOm Catalysts for Dry Reforming of Methane [J]. Catalysts, 2019, 9 (12): 1055.

 doi:10.20944/preprints202412.1624.v1

21. Li X., Zhao Z.-J., Zeng L., et al. On the role of Ce in CO2 adsorption and activation over lanthanum species [J]. Chemical Science, 2018, 9 (14): 3426-3437.
22. Jin B., Li S., Liu Y., et al. Engineering metal-oxide interface by depositing ZrO2 overcoating on Ni/Al2O3 for dry reforming of methane [J]. Chemical Engineering Journal, 2022, 436: 135195.
23. Diao Y. A., Zhang X., Liu Y., et al. Plasma-assisted dry reforming of methane over Mo2CNi/Al2O3 catalysts: Effects of beta-Mo2C promoter [J]. Applied Catalysis B-Environmental, 2022, 301: 120779.
24. Liu H., He D. Properties of Ni/Y2O3 and its catalytic performance in methane conversion to syngas [J]. International Journal of Hydrogen Energy, 2011, 36 (22): 14447-14454.
25. Strnisa F., Sagar V. T., Djinovic P., et al. Ni-containing CeO2 rods for dry reforming of methane: Activity tests and a multiscale lattice Boltzmann model analysis in two model geometries [J]. Chemical Engineering Journal, 2021, 413: 127498.
26. Wang F., Cai W., Provendier H., et al. Hydrogen production from ethanol steam reforming over Ir/CeO2 catalysts: Enhanced stability by PrOx promotion [J]. International Journal of Hydrogen Energy, 2011, 36: 13566-13574.
27. Dilawar Sharma N., Singh J., Vijay A., et al. Investigations of anharmonic effects via phonon mode variations in nanocrystalline Dy2O3 , Gd2O3 and Y2O3 [J]. Journal of Raman Spectroscopy, 2017, 48: 822-828.
28. Fang X., Xia L., Li S., et al. Superior 3DOM Y2Zr2O7 supports for Ni to fabricate highly active and selective catalysts for CO2 methanation [J]. Fuel, 2021, 293: 120460.
29. Xia L., Fang X., Xu X., et al. The promotional effects of plasma treating on Ni/Y2Ti2O7 for steam reforming of methane (SRM): Elucidating the NiO-support interaction and the states of the surface oxygen anions [J]. International Journal of Hydrogen Energy, 2020, 45 (7): 4556-4569.
30. Silva R. S., Cunha F., Barrozo P. Raman spectroscopy of the Al-doping induced structural phase transition in LaCrO3 perovskite [J]. Solid State Communications, 2021: 114346.
31. Triyono D., Hanifah U., Laysandra H. Structural and optical properties of Mg-substituted LaFeO3 nanoparticles prepared by a sol-gel method [J]. Results in Physics, 2020, 16: 102995.
32. Xie Y., Xie F., Wang L., et al. Efficient dry reforming of methane with carbon dioxide reaction on Ni@Y2O3 nanofibers anti-carbon deposition catalyst prepared by electrospinning-hydrothermal method [J]. International Journal of Hydrogen Energy, 2020, 45: 31494-31506.
33. Sun J., Luo D., Xiao P., et al. High yield hydrogen production from low CO selectivity ethanol steam reforming over modified Ni/Y2O3 catalysts at low temperature for fuel cell application [J]. Journal of Power Sources, 2008, 184: 385-391.
34. Fang X., Xia L., Peng L., et al. Ln2Zr2O7 compounds (Ln = La, Pr, Sm, Y) with varied rare earth A sites for low temperature oxidative coupling of methane [J]. Chinese Chemical Letters, 2019, 30: 1141-1146.
35. Pereñiguez R., Gonzalez-delaCruz V. M., Caballero A., et al. LaNiO3 as a precursor of Ni/La2O3 for CO2 reforming of CH4: Effect of the presence of an amorphous NiO phase [J]. Applied Catalysis B: Environmental, 2012, 123-124: 324-332.
36. Nurk G., Kooser K., Urpelainen S., et al. Near ambient pressure X-ray photoelectron - and impedance spectroscopy study of NiO-Ce0.9Gd0.1O2-δ anode reduction using a novel dualchamber spectroelectrochemical cell [J]. Journal of Power Sources, 2018, 378: 589-596.
37. Oemar U., Hidajat K., Kawi S. High catalytic stability of Pd-Ni/Y2O3 formed by interfacial Cl for oxy-CO2 reforming of CH4 [J]. Catalysis Today, 2017, 281: 276-294.
38. Singha R. K., Shukla A., Yadav A., et al. Effect of metal-support interaction on activity and stability of Ni-CeO2 catalyst for partial oxidation of methane [J]. Applied Catalysis B: Environmental, 2016, 191: 165-178.
39. Singha R. K., Yadav A., Agrawal A., et al. Synthesis of highly coke resistant Ni nanoparticles supported MgO/ZnO catalyst for reforming of methane with carbon dioxide [J]. Applied Catalysis B: Environmental, 2016, 202: 473-488.
40. Zhang M., Zhang J., Zhou Z., et al. Effects of the surface adsorbed oxygen species tuned by rare-earth metal doping on dry reforming of methane over Ni/ZrO2 catalyst [J]. Applied Catalysis B: Environmental, 2019, 264: 118522.

 doi:10.20944/preprints202412.1624.v1

41. Fan, Yuqiao, Miao, et al. Oxidative coupling of methane over Y2O3 and Sr–Y2O3 nanorods [J]. Reaction Kinetics, Mechanisms and Catalysis, 2021, 134: 711-725.
42. Zeng R., Jin G., He D., et al. Oxygen vacancy promoted CO2 activation over acidic-treated LaCoO3 for dry reforming of propane [J]. Materials Today Sustainability, 2022, 19: 100162.
43. Yang J., Hu S., Fang Y., et al. Oxygen Vacancy Promoted O2 Activation over Perovskite Oxide for Low-Temperature CO Oxidation [J]. ACS Catalysis, 2019, 11: 9757-9763.
44. Fei Z., He S., Li L., et al. Morphology-directed synthesis of Co3O4 nanotubes based on modified Kirkendall effect and its application in CH4 combustion [J]. Chemical Communications, 2012, 48: 853-855.
45. Xu J., Xi R., Zhang Z., et al. Promoting the surface active sites of defect BaSnO3 perovskite with BaBr2 for the oxidative coupling of methane [J]. Catalysis Today, 2020, 374: 29-37.
46. Long R. Q., Wan H. L. In situ confocal microprobe Ramanspectroscopy study of CeO2/BaF2 catalyst for theoxidative coupling of methane [J]. Journal of the Chemical Society, Faraday Transactions, 1997, 93: 355-358.
47. Abd Ghani N. A., Azapour A., Syed Muhammad A. F. a., et al. Dry reforming of methane for hydrogen production over NiCo catalysts: Effect of NbZr promoters [J]. International Journal of Hydrogen Energy, 2018, 44: 20881-20888.
48. Solis-Garcia A., Louvier-Hernandez J. F., Almendarez-Camarillo A., et al. Participation of surface bicarbonate, formate and methoxy species in the carbon dioxide methanation catalyzed by ZrO2-supported Ni [J]. Applied Catalysis B: Environmental, 2017, 29: 3-7.
49. Zhang S., Ying M., Yu J., et al. NixAl1O2-δ mesoporous catalysts for dry reforming of methane: The special role of NiAl2O4 spinel phase and its reaction mechanism [J]. Applied Catalysis B: Environmental, 2021, 291: 120047